

Article

Lean Methane Mixtures in Turbulent Jet Ignition Combustion System

Ireneusz Pielecha *  and Filip Szwajca 

Faculty of Civil and Transport Engineering, Poznan University of Technology, 60-965 Poznan, Poland

* Correspondence: ireneusz.pielecha@put.poznan.pl

Abstract: The development of modern vehicle drives is aimed at reducing fuel consumption (i.e., crude oil) and minimizing the exhaust emission of toxic components. One such development is the implementation of a two-stage combustion system. Such a system initiates ignition in the prechamber, and then the burning mixture flows into the main chamber, where it ignites the lean mixture. The system allows the efficient combustion of lean mixtures, both liquid and gaseous fuels, in the cylinder. This article proposes a solution for internal combustion engines with a cylinder capacity of approx. 500 cm³. The tests were carried out on a single-cylinder engine powered by pure methane supplied through a double, parallel injection system. A wide range of charge ignitability requires the use of an active chamber containing an injector and a spark plug. The tests were carried out at $n = 1500$ rpm with three load values (indicated mean effective pressure, IMEP): 2, 4 and 6 bar. All of these tests were carried out at a constant value of the center of combustion (CoC), 8 deg CA. This approach resulted in the ignition timing being the control signal for the CoC. As a result of the conducted research, it was found that an increase in the load, which improved the inter-chamber flow, allowed for the combustion of leaner mixtures without increasing the coefficient of variation, CoV(IMEP). The tests achieved a lean mixture combustion with a value of $\lambda = 1.7$ and an acceptable level of non-uniformity of the engine operation, $\text{CoV(IMEP)} < 8\%$. The engine's indicated efficiency when using a two-stage system reached a value of about 42% at $\lambda = 1.5$ (which is about 8 percentage points more than with a conventional combustion system at $\lambda = 1.0$).

Keywords: combustion system; turbulent jet ignition; prechamber; combustion efficiency; CNG engine



Citation: Pielecha, I.; Szwajca, F. Lean Methane Mixtures in Turbulent Jet Ignition Combustion System. *Energies* **2023**, *16*, 1236. <https://doi.org/10.3390/en16031236>

Academic Editor: Venera Giurcan

Received: 30 December 2022

Revised: 12 January 2023

Accepted: 20 January 2023

Published: 23 January 2023



Copyright: © 2023 by the authors. Licensee MDPI, Basel, Switzerland. This article is an open access article distributed under the terms and conditions of the Creative Commons Attribution (CC BY) license (<https://creativecommons.org/licenses/by/4.0/>).

1. Introduction

Modern powertrain development is focused on (1) maximizing specific power and (2) minimizing the exhaust emission of harmful compounds. One of the decisive factors shaping the development of drives is the reduction of fuel consumption while reducing carbon dioxide emissions. Article 4 of Regulation (EC) No 443/2009 and Article 4 of Regulation (EU) No 510/2011 requires manufacturers of new passenger cars to comply with certain levels of CO₂ emissions. Until 2015, the average CO₂ emission value of the vehicle fleet was 130 g/km [1]. Since 2021, this value has become 50 g/km [2]. Further reductions in this emission value are being pursued through the use of alternative fuels or the development of new combustion systems for light- and medium-duty non-zero-emission vehicles [3]. The ACEA report indicates that in 2021, conventional fuels (petrol and diesel) still dominated the market with a 60% share [4]. In April 2019, the European Parliament and Council adopted Regulation (EU) 2019/631, introducing CO₂ emission standards for new passenger cars and light commercial vehicles (vans) in the European Union. This regulation set reduction targets of −15% and −37.5% for the tailpipe CO₂ emissions of newly registered cars for 2025 and 2030 respectively. The 2030 target set for vans was −31% [5]. As part of the development of combustion systems, new solutions are being developed such as homogeneous charge combustion systems (HCCI) [6,7] or

reactivity charge compression ignition (RCCI) [8,9], commonly referred to as diesel low-temperature combustion (LTC) [10,11]. All of these systems only partially reduce particulate or nitrogen oxide emissions (Figure 1).

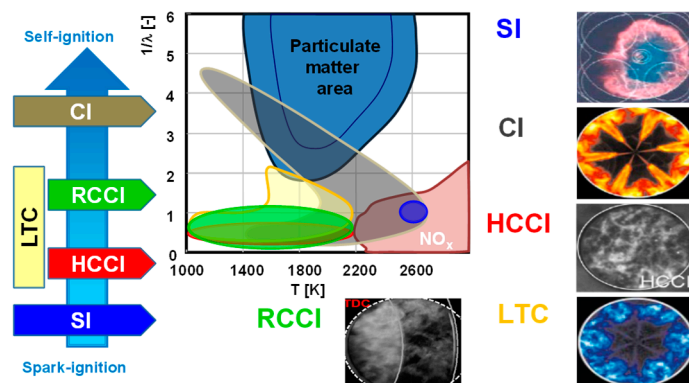


Figure 1. Modern combustion systems and the possibilities of reducing exhaust emissions [12–14].

One of the measures used to reduce fuel consumption and exhaust emissions is a two-stage combustion system, turbulent jet ignition [15]. This system has been in development since the 1950s [16]. It relies on using a prechamber, which significantly improves the thermodynamic parameters of the combustion process in terms of lean mixture combustion compared to the conventional SI system or even the use of a prechamber spark plug [17]. The effects of using the TJI system depend on the geometry of the ignition chamber and the mixture formation system used [18,19]. Two systems can be distinguished in the system: a passive and active prechamber (Figure 2). In the case of an active prechamber, an additional dose of fuel is delivered directly to the spark plug area. In such a system, it is possible to use the widespread indirect injection of natural gas or direct injection, which is under development. In addition, it is possible to use both simultaneously.

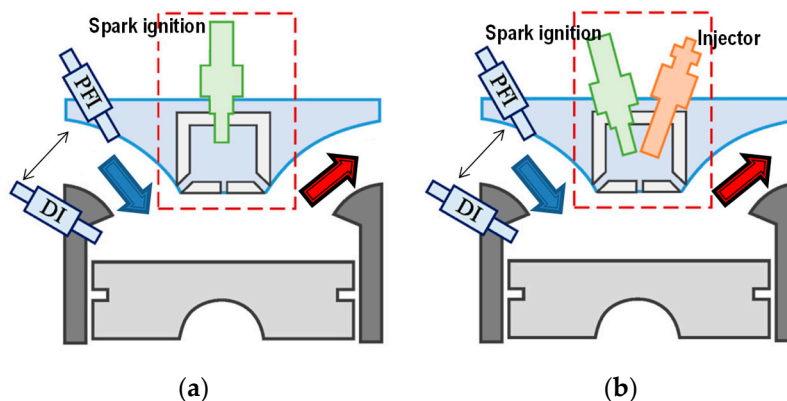


Figure 2. Two-stage combustion systems: (a) Passive prechamber; (b) Active prechamber [20].

Studies conducted with the use of prechambers have indicated the possibility of obtaining about a 2–9% reduction in fuel consumption [21].

In the article, IMEP denotes the indicated mean effective pressure, while BMEP stands for the break mean effective pressure. Sens and Binder [21], conducting research on prechambers, pointed out differences in the combustion process when using active and passive chambers. The tests were carried out at $n = 1500$ rpm and $BMEP = 6$ bar. The passive chamber enables the combustion of lean mixtures at the maximum value of $\lambda = 1.5$. Making the mixture even leaner is only possible with the use of an active chamber. The combustion process was maintained up to the excess air coefficient value of $\lambda = 2.3$. With this value of λ , the coefficient of variation became 5%. The use of a passive chamber caused the stability of the operation at the level of $CoV(IMEP) = 5\%$ to already occur at $\lambda = 1.4$.

It was also found that the combustion at a crankshaft angle of 10–70 deg increases as the mixture becomes leaner. Whether the initial combustion time (AI10–50) or final combustion time (AI50–90) increases or not has not been analyzed (angle of 10 or 50% mass burn fuel, AI10 or AI50).

Studies with active and passive chambers were conducted by Soltik and Hilfiker [22]. In the research, they used methane and a mixture of methane and hydrogen (3.5% mass H₂; 8% energy) to power the engine. They found that the active chamber allowed the combustion of charges up to $\lambda = 1.7$ (pure methane) and $\lambda = 1.9$ (mixture: methane + hydrogen). The active chamber enabled the process for values up to $\lambda = 2.1$ (pure methane) or $\lambda = 2.2$ (methane + hydrogen).

Research conducted by Liu et al. [23] more effectively confirmed the performance indicators of the system with an active chamber. The tests used a constant-volume combustion chamber. It was powered with methane and hydrogen in the ranges of $\lambda = 1.0$ –1.8 (methane) and $\lambda = 1.0$ –5.0 (hydrogen). The use of an active chamber (methane, at $\lambda = 1.4$) resulted in an earlier start of the combustion process and increased the process intensity ($dp/d\alpha$). Mixtures with a value of $\lambda > 1.4$ did not ignite when using the passive chamber. When fueling with hydrogen, combustion was obtained at $\lambda = 4.0$ (methane; very slow combustion) and $\lambda = 5.0$ in the active chamber (hydrogen; slow combustion).

The coefficient of variation CoV [24] is one of the indicators determining the variability of engine operation. It is most often used to determine the variability of the IMEP [25], but it is also possible to use it to determine the variability of the 50% combustion location (AI50), combustion duration, peak pressure and its location, and the maximum rate of pressure rise and its location [26].

Therefore, the CoV(IMEP) is used to evaluate the combustion stability of a typical engine. The CoV(IMEP) is the ratio of the standard deviation of p_i to the averaged p_i over 100 continuous working cycles, and CoV(IMEP) generally cannot exceed 5% [27,28]. Often in RCCI engines, the CoV(IMEP) value exceeds 5% [27]. In the tests of the hydrogen-powered engine conducted by [28], at a high excess air ratio ($\lambda > 3.2$), the CoV(IMEP) value exceeded 6%.

Most of the research conducted so far concerns engines and work indicators, as well as exhaust emissions reduction. The current research focuses on determining the unevenness of the engine operation relative to a variable prechamber fuel dose; however, it assumes a constant value of the CoC. The center of combustion (CoC) is defined as the angle of the crankshaft at which 50% of the fuel mass has been burned, and is also designated as CA50. This methodology makes the ignition angle control an executive element used to obtain the desired CoC settings. Such a method of controlling the combustion process has also been used by other researchers [29–31].

Other methods are based on obtaining the peak combustion pressure at a specific crankshaft angle. The new methodology takes into account the quality of the combustion process and engine operation irregularities, as the setting values are determined based on the many operating cycles ($n = 100$ cycles). The pressure curves presented in the paper are averaged from the above 100 cycles and marked P_{av} , and the maximum value is P_m .

The article focuses on the thermodynamic parameters of the two-stage combustion process of a lean methane mixture. The effect of the control parameters on the engine operating stability was analyzed. Additionally, the energetic indicators of operation were determined. The fuel dose distribution method between combustion chambers is also presented. It is a key issue due to the wide range of excess air ratio values used. The identification of inter-chamber flows and their changes relative to engine operating points is also addressed.

2. Materials and Methods

The two-stage combustion process tests were carried out according to the diagram shown in Figure 3. The AVL 5804 research combustion engine, modified for the use of gaseous fuel, was equipped with a methane supply system (in the intake duct and

prechamber). The Micro Motion ELITE CMFS010M Coriolis Meter gas flow meter (with a measuring range of 0.1–2 kg/h) was used in the injection system in the intake tract, and Bronkhorst 111B (with a measuring range of 0.1–100 g/h) for small doses of gas in the prechamber. Pressure sensors were used in both combustion chambers (in the main chamber: AVL GH14D; and in the prechamber: Kistler M3.5). Engine operating parameters were recorded using the AVL IndiSmart system (with a resolution of 0.1 deg CA).

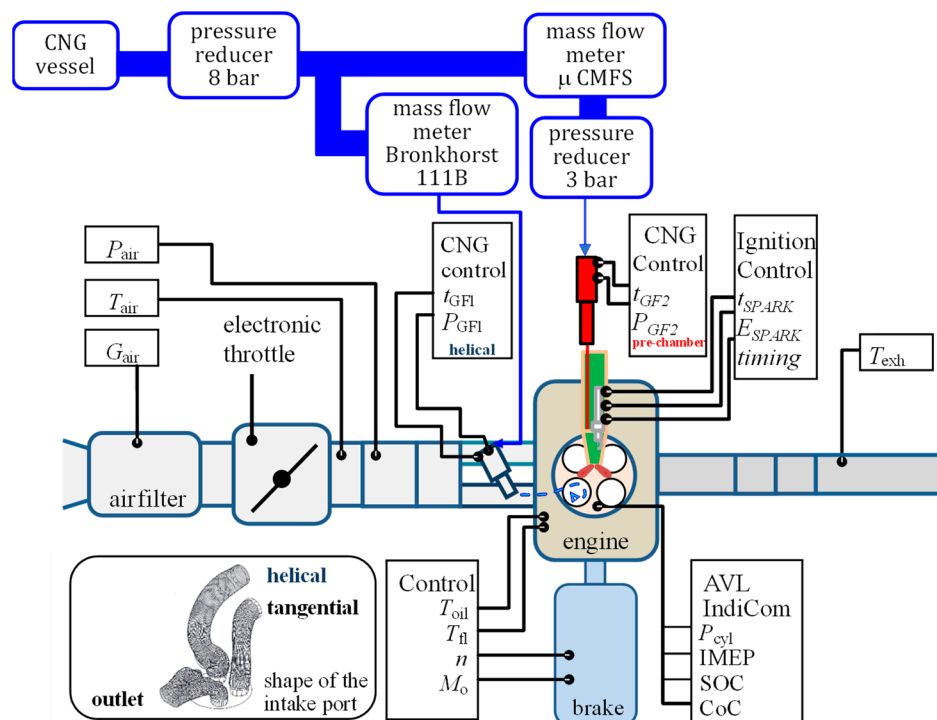


Figure 3. Schematic of the measurement system analysis for the two-stage combustion system with the AVL 5804 engine and the apparatus for engine indication and exhaust emission analysis.

A throttle with a diameter of 28 mm was used to regulate the air intake (without the supercharging system). The throttle was controlled using an open Engine Management Unit—EMU Black by Ecumaster. The ignition system in the prechamber (active prechamber) was a Beru pencil coil. The coil control enabled setting both the coil charging time ($t_{coil} = 3$ ms) and the ignition advance time using the M10 spark plug.

The ongoing value of the excess air coefficient was set in accordance with the indications of fuel consumption (in both chambers) and air consumption. The measurement was based on the fuel components, not on the amount of oxygen in the exhaust gas.

The engine was equipped with two injection systems (Figure 4) supplied at a pressure of $p = 8$ bar to the intake system (PFI) and 3 bar to the prechamber (DI). The pressure was differentiated due to the requirements as to the size of fuel doses delivered separately to the PC (preliminary chamber) and MC (main chamber). A constant start of fuel injection was established at the angle $\alpha = 240$ deg bTDC (for both injectors). The fuel dose was controlled by the injection time, which was significantly greater when injected into the intake port. Figure 4 shows the location of the two injectors (to the prechamber and to the inlet channel).

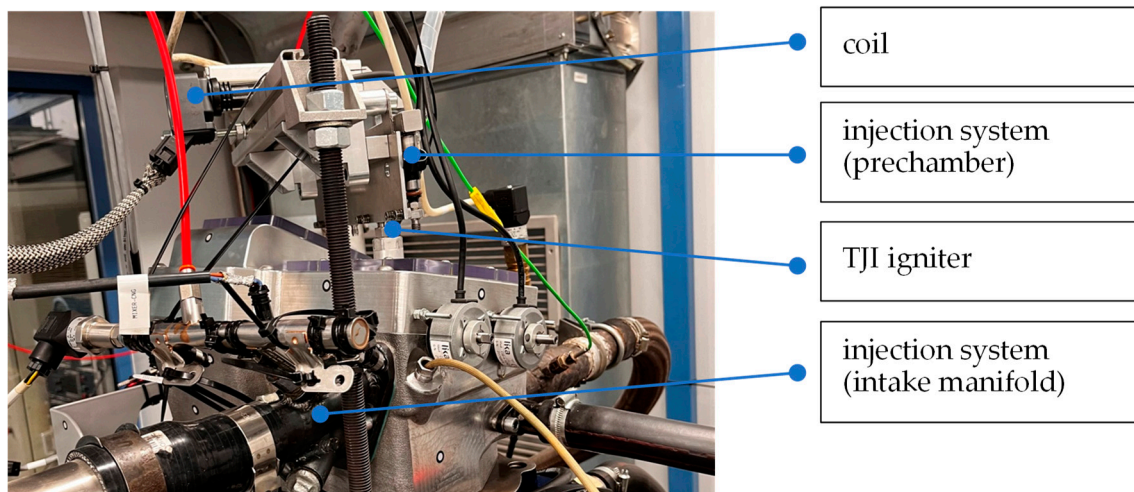


Figure 4. Image of two gas supply systems: (1) to the prechamber and (2) to the intake duct.

The combustion chamber was equipped with a prechamber with a volume of 2.29 cm^3 . This value accounted for 0.45% of the total engine stroke volume (at BDC) and 6.6% of the capacity (at TDC). The prechamber was equipped with an M10 spark plug and a gas supply (Figure 5a). The prechamber had 6 holes as shown in Figure 5b. Other sizes of the prechamber are listed in Table 1.

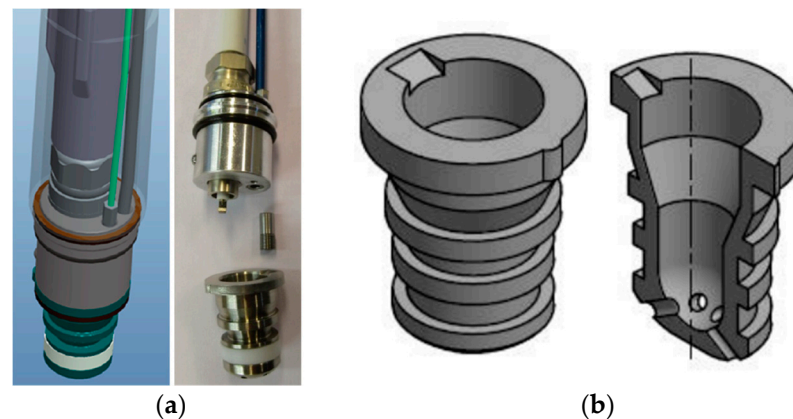


Figure 5. Solutions of direct gas supply system to the prechamber: (a) spark plug and a return valve system [32]; (b) the prechamber used in the current study.

Table 1. Technical specifications of the prechamber used in research.

Parameter	Unit	Value
Number of holes	-	6
Hole diameter	mm	1.7
Spark plug		M10
V_{PC}/V_{ss}	$-\text{/cm}^3$	$2.29/510 \rightarrow 0.45\%$ (max) $2.29/35.1 \rightarrow 6.5\%$ (min)

A single-cylinder AVL 5804 test engine was used; its technical specifications are listed in Table 2. The engine was equipped with an independent conditioning system for the cooling fluid and oil, called AVL 577. The AVL AMK DW13-170 asynchronous engine was used for the engine load.

Table 2. Technical data of the single-cylinder test engine used.

Parameter	Unit	Value
Engine	–	1-cyl., 4-valve, SI, TJI
Displacement	dm ³	0.5107
Bore × stroke	mm	85 × 90
Compression ratio	–	15.5
Fueling	–	DI and PFI (EM injectors)
Air system	–	Naturally aspirated

The tests of the two-stage combustion system fueled with methane were carried out for three engine load values with the excess air coefficient ranging from $\lambda = 1.0$ (no fuel injection into the prechamber) to $\lambda = 1.8$ at $n = 1500$ rpm. During the injection of fuel into the prechamber, the following relationship was maintained:

$$q_{PC} + q_{MC} = \text{const} \quad (1)$$

where q_{PC} and q_{MC} indicate the fuel dose in the prechamber and the main chamber.

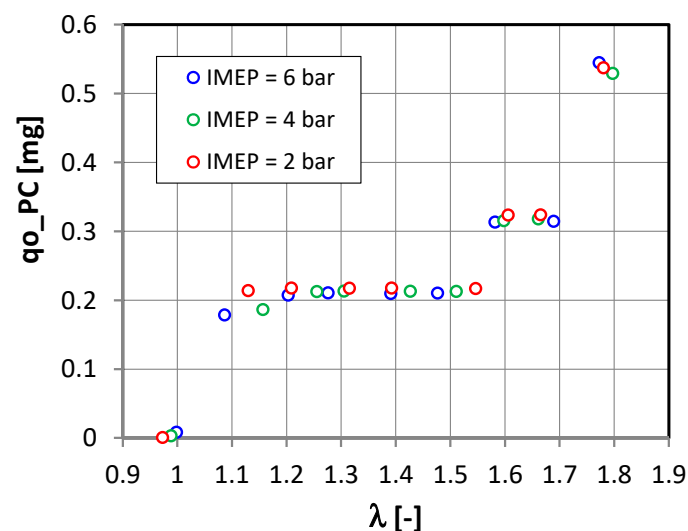
During the tests, the assumption was made that the ignition angle will be the control value to be adjusted to achieve a constant CoC value:

$$\alpha_{ia} = f(\text{IMEP}, \lambda) = \text{var} \rightarrow \text{CoC} = \text{const} \quad (2)$$

where the center of combustion is defined as the crankshaft angle at which 50% of the heat is released (the CoC value was determined to be 8 deg aTDC) [33]:

$$\text{CoC} = \alpha \text{ at } 0.5 \times \int_{\text{SOC}}^{\text{EOC}} \frac{dQ_{\text{net}}}{d\theta} d\theta \quad (3)$$

The tests were carried out with a constant fuel dose (Figure 6) and a varied air dose (adjustable throttle), regardless of the average indicated pressure value. Such variability of the tests made it possible to evaluate the engine efficiency, the increase in which indicated an improvement in the combustion process. Preliminary studies have found that increasing the prechamber dose in the lean mixture range contributes to the improvement of the combustion process quality, as well as to the assumptions presented in Equations (1) and (2). Regarding the combustion of near-stoichiometric mixtures, fuel dosing to the PC deteriorated engine operation.

**Figure 6.** Test conditions: prechamber fuel dose values as a function of the engine load.

Gaseous fuel was supplied to the engine via two systems (Figure 7): (a) the first was a low-pressure injection into the intake manifold; (b) the second was also a low-pressure injection but into the prechamber. Data in Figure 6 indicate early fuel injection into the intake manifold. The start of fuel injection was 240 deg bTDC. Prechamber injection also started at 240 deg bTDC. The gas pressure values in the system were different ($P_{INJ_PC} < P_{INJ_MC}$). For this reason, the prechamber fuel dose was significantly lower than that fed into the intake manifold.

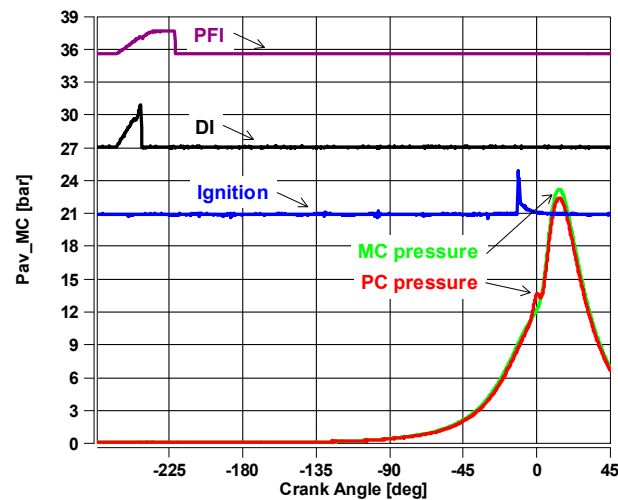


Figure 7. The fuel supply parameters relative to the ignition time and the combustion process.

Early injection into the prechamber caused some of the gaseous fuel to enter the cylinder. At the same time, fuel was injected into the cylinder through the intake manifold. These conditions resulted in a specific (but not measured) excess air ratio in the prechamber.

3. Inter-Chamber Flows Analyses

The change in the fuel dose fed into the prechamber was also associated with inter-chamber flows (Figure 8). The analysis of the inter-chamber flows (blue lines) for different values of IMEP is shown in the background of the pressure waveform in the chambers of the system at a load of 2 bar.

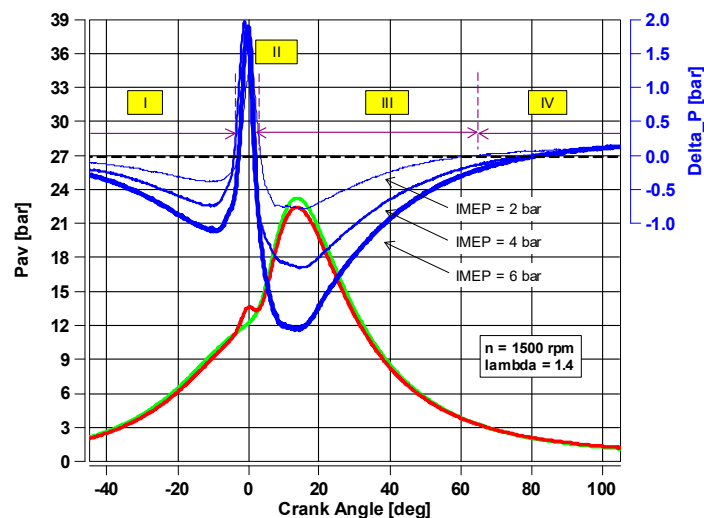


Figure 8. Analysis of pressure changes in combustion chambers: the inter-chamber flows (red line—cylinder pressure; green line—prechamber pressure).

At low values of the IMEP values, the mixture flowed into the main chamber (phase I in Figure 8). Then, during compression, it flowed into the prechamber (phase II in Figure 8). Ignition of the mixture in the prechamber caused the mixture to flow into the main chamber. In the final phase of the outflow, the pressure in the prechamber reached higher values than in the main chamber (phase IV; Figure 8). Increasing the average IMEP did not change the nature of the flow. However, an increase in IMEP caused an increase in the pressure difference (ΔP ; Figure 8). Based on the flow analysis, it was found that increasing IMEP caused an increase in the pressure difference, while maintaining a constant pressure in the prechamber (area II; Figure 8). A small angular change in the flows resulted from the need to maintain a constant CoC value (Equation (2)).

4. Engine Thermodynamic Performance Indicators

A complete analysis of the pressure curve in the cylinder is shown in Figure 9. As previously mentioned, the excess air ratio was adjusted by changing the amount of intake air (at a constant fuel dose). The thick line shows the changes in pressure in the cylinder at $\lambda = 1.0$. The dashed line indicates the pressure in the cylinder at $\lambda = 1.8$. Points (a) and (b) mark the course of pressure in the cylinder (MC) and in the ignition chamber (PC), respectively. There is an apparent shift in the prechamber start of combustion towards earlier ignition angles in order to maintain a constant CoC value.

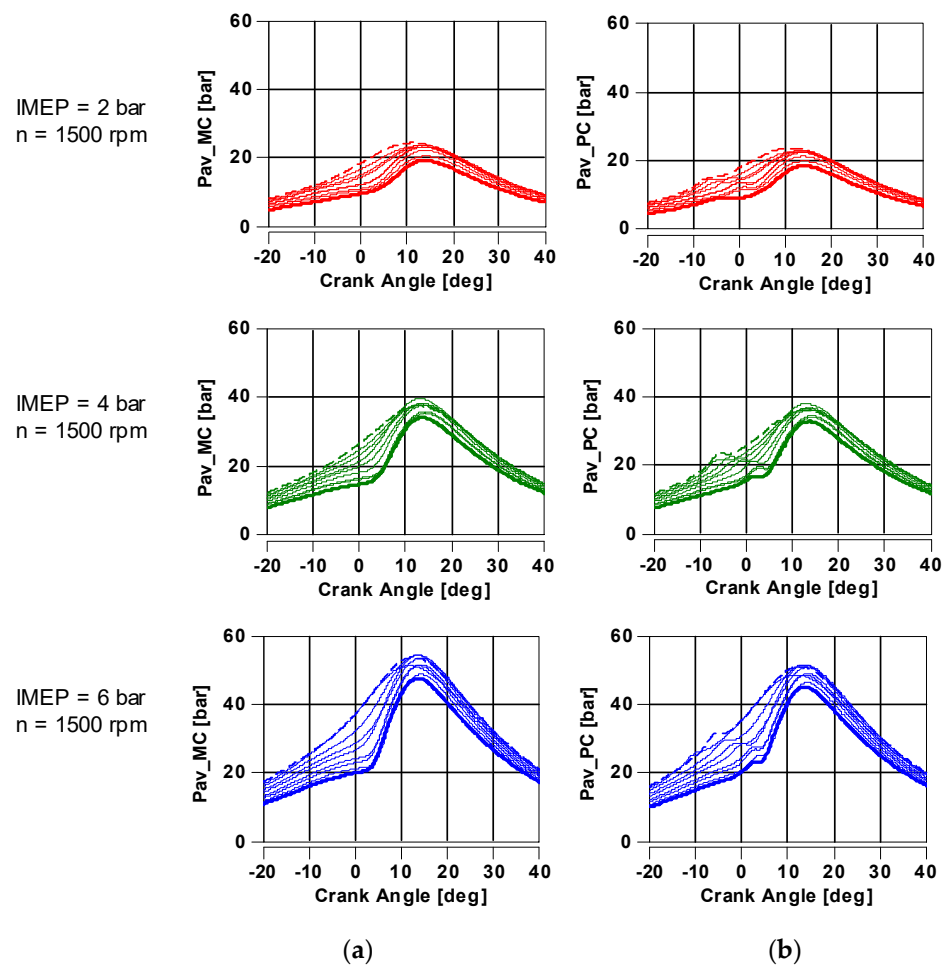


Figure 9. Pressure value in the cylinder: (a) in the main chamber; (b) in the prechamber.

Changing the value of the excess air coefficient caused the start of combustion to be advanced (due to the necessity to meet condition (2)) depending on the average indicated pressure:

- (a) at IMEP = 2 bar: SOC_{PC} = 6 to 0 CA deg bTDC,
- (b) at IMEP = 4 bar: SOC_{PC} = 6 to 2 CA deg bTDC,
- (c) at IMEP = 6 bar: SOC_{PC} = 10 to 2 CA deg bTDC.

While researching the combustion process, 100 consecutive cycles of engine operation were analyzed. The engine operation uniformity analysis was carried out using the CoV(IMEP) non-uniformity coefficient. Figure 10 shows selected engine operating points (at various λ -values) at the constant engine load value of IMEP = 2 bar. The blue dots indicate the maximum pressure value in subsequent cycles. It should be noted that this coefficient was determined with small load values that were characterized by high variability of engine operation. The conducted analyses indicated the existence of small changes in CoV(IMEP) values below 2%. This means that despite the large values of the difference between the extreme peak pressure Pmx values, the changes in CoV(IMEP) were small.

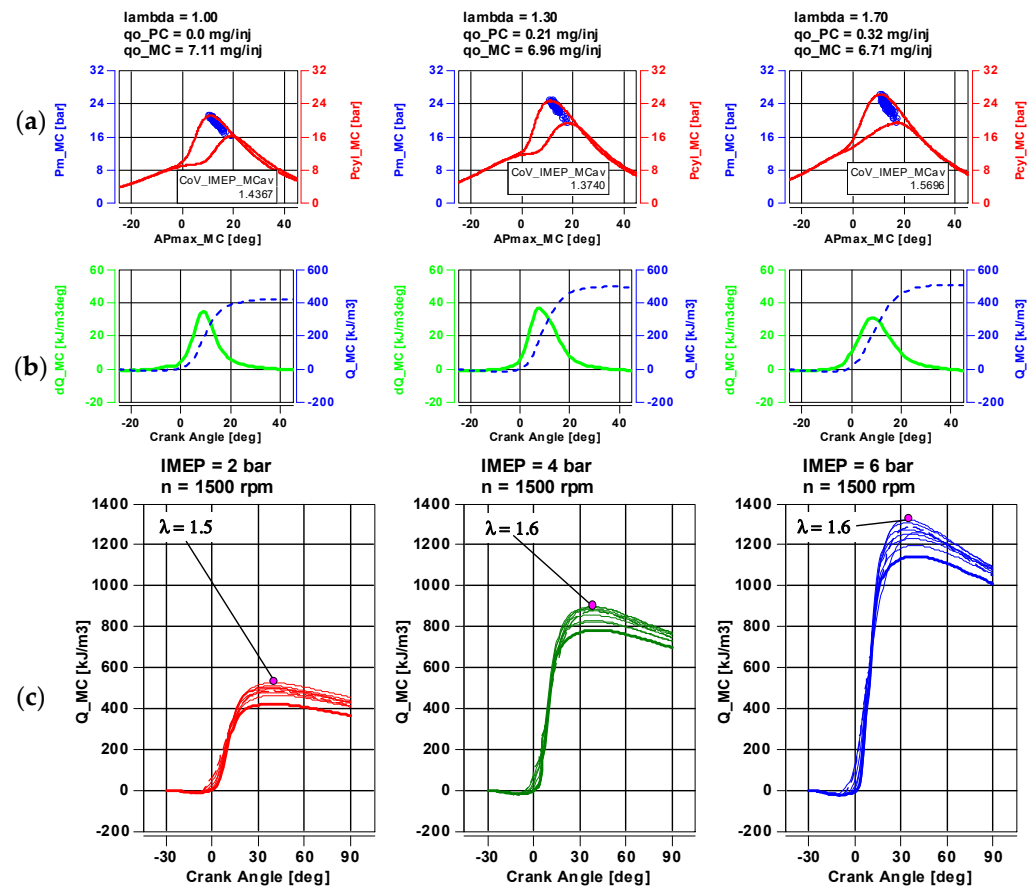


Figure 10. Evaluation of the combustion process at IMEP = 2 bar: (a) changes in the extreme combustion pressure values based on the maximum combustion pressure values; (b) the heat release rate curve and its value; (c) the heat release rate curve for all IMEP values and its maximum-value.

The net heat release rate (without heat loss) is determined by applying the first law of thermodynamics using the following equation:

$$dQ = \frac{dQ_{net}}{d\alpha} = \frac{\gamma}{\gamma - 1} p \frac{dV}{d\alpha} + \frac{1}{\gamma - 1} V \frac{dp}{d\alpha}, \quad (4)$$

and heat release is given by:

$$Q = \int_{SOC}^{EOC} \frac{dQ_{net}}{d\alpha} d\alpha, \quad (5)$$

where p is the instantaneous cylinder pressure, α is the crank angle, γ is the ratio of the specific heats and V is the instantaneous cylinder volume. The instantaneous cylinder volume was calculated from the engine geometry and crank angle values.

The analysis of the heat release rate indicates the best combustion process curve (among those presented) at $\lambda = 1.3$ (Figure 10b). As the excess air coefficient increased, higher values of the amount of released heat could be observed. This indicated an increase in the overall engine efficiency, which at the same time indicated the possibility of reducing fuel consumption. This reduction in fuel consumption resulted from the high value of the excess air coefficient and the simultaneous increase in the amount of heat released. The heat release rate curve for all IMEP values and its maximum value are presented in Figure 10c.

5. Stability of Engine Operation

The cylinder peak pressure analysis (averaged over 100 work cycles; Figure 11a) indicated that the maximum value was obtained with an excess air coefficient between $1.3 > \lambda > 1.6$. The fact that lower values could be observed for the prechamber is characteristic for this setup. This was also confirmed by the data in Figure 8. The comparison of the specific indicated fuel consumption (Figure 11b) pointed to the existence of a minimum for lean mixtures in the range of $1.5 < \lambda < 1.6$. An increased engine load indicated a specific indicated fuel consumption of less than 180 g/kWh. This means that the maximum motor efficiency values could also be expected in this range.

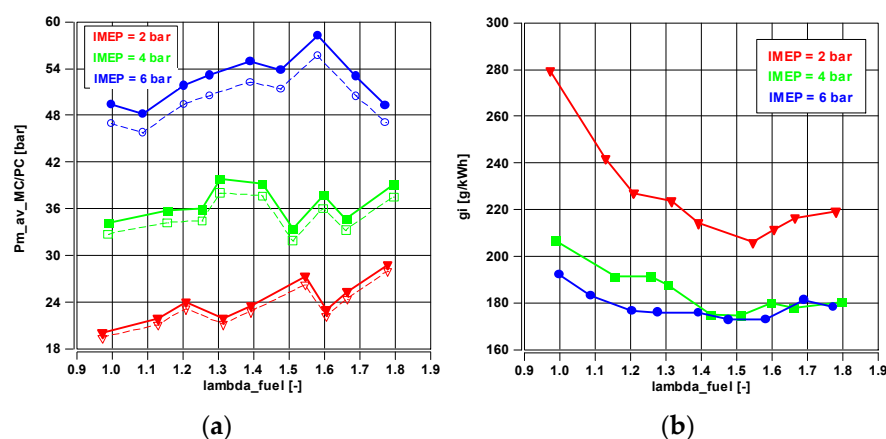


Figure 11. Operating indicators of the tested engine: (a) average maximum pressure values in the main chamber and in the prechamber; (b) specific indicating fuel consumption vs. λ -value.

Figure 12 shows the engine operation variability analysis. The presented data refer to the prechamber and the main chamber. They show that the largest values of work variability fell within $1.0 < \lambda < 1.2$ at IMEP = 2 bar. These values may have resulted from the start of the injection of fuel into the prechamber. This indicates a deterioration of the combustion process in the prechamber due to low air flow values or limited inter-chamber flow. Increasing the amount of air (at the same fuel dose) resulted in an improvement in the combustion process quality, as indicated by a sharp reduction in CoV(IMEP). It is worth noting that in the range $\lambda = 1.2$ – 1.6 , the value of CoV(IMEP) was $< 2\%$. Such values indicate a very good combustion process quality and high repeatability of the engine's work cycle. A further increase in the excess air coefficient (charge depletion) led to an increase in variable and uneven operation and it reached its maximum values at $\lambda = 1.8$ (CoV(IMEP) $\sim 10\%$). Increasing the engine load value caused no increase in CoV(IMEP) in the range of small excess air coefficient values. A characteristic element is the operation of the engine with a high excess air coefficient. Regardless of the engine load, an increase in CoV(IMEP) was observed, where it reached values of up to 10%.

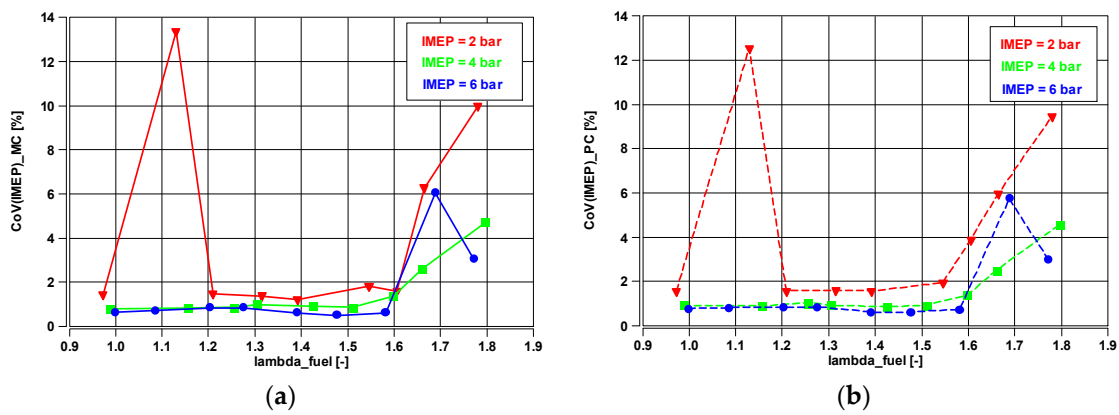


Figure 12. Non-uniformity of the indicated mean engine pressure for different values of fuel mixture leanness: (a) in the main chamber; (b) in the prechamber.

The so-called return maps are widely used in dynamic problems. They help visualize the current and next engine cycle. Using them widely together with the coefficient of variation (CoV) in engine processes has been demonstrated in many other papers [34–36].

Return maps are shown in Figure 13. The small dispersion of the maximum pressure value in subsequent work cycles resulted in a large concentration of points in a small area.

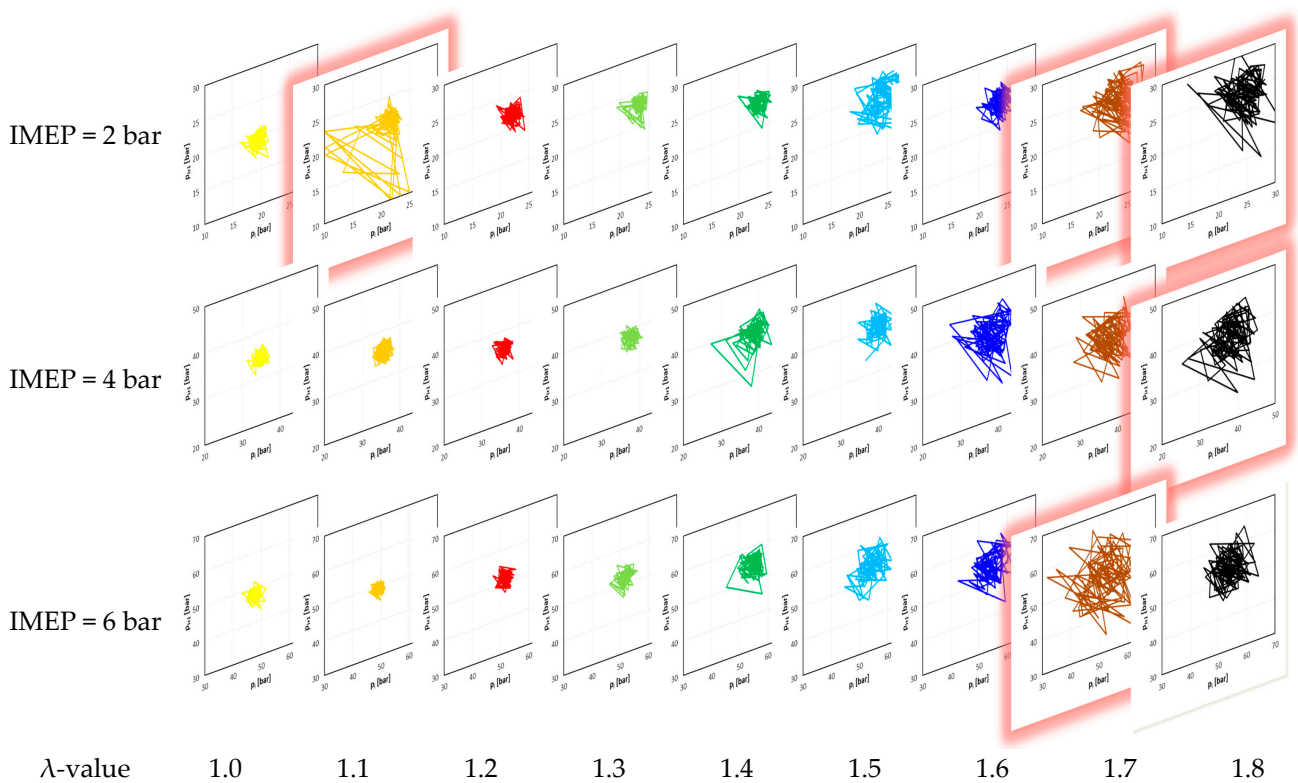


Figure 13. Analysis of work cycles in return map format for various engine load values for $n = 1500$ rpm.

The reverse map version enabled the imaging of successive cycles, and the coefficients of variation were quantified only by the result of this dispersion. For this reason, maps make it possible to “track” uneven and variable engine operation. A large scattering of successive work cycles caused the areas in Figure 12 to occupy more space. For this reason, the largest scatters of the maximum combustion pressure values are additionally marked. It shows that a large variability in these parameters especially occurred in the range of low

load and high excess air coefficient values (IMEP = 2 bar). Large variability values also occurred at other values of IMEP. The figure is only a qualitative view of the issue of engine operation stability. Therefore, a detailed analysis in the form of a two-dimensional system was not performed.

Large variability at IMEP = 2 and at $\lambda = 1.1$ may have resulted from a change in the power supply method: the switch from the passive chamber system to the active chamber. In the case of a small engine load, the velocities of inter-chamber flows were quite small, which caused large changes in the excess air coefficient in the prechamber. Such results may be an excuse not to use the two-stage system for small engine loads and $\lambda \sim 1$.

The engine work variability assessment was also made in relation to the engine load map. The variability was found to be lower in the main chamber than in the prechamber. This was particularly evident when increasing the excess air coefficient (Figure 14). Up to $\lambda < 1.4$, the CoV(IMEP) value was almost the same, regardless of the engine load. Increasing the value of λ created a very lean mixture in the prechamber that failed to ignite properly. Such behavior resulted in high operation variability (CoV(IMEP) > 5%). Such values indicate the need to limit the excess air coefficient above $\lambda > 1.6$, because then CoV(IMEP) > 5.5%.

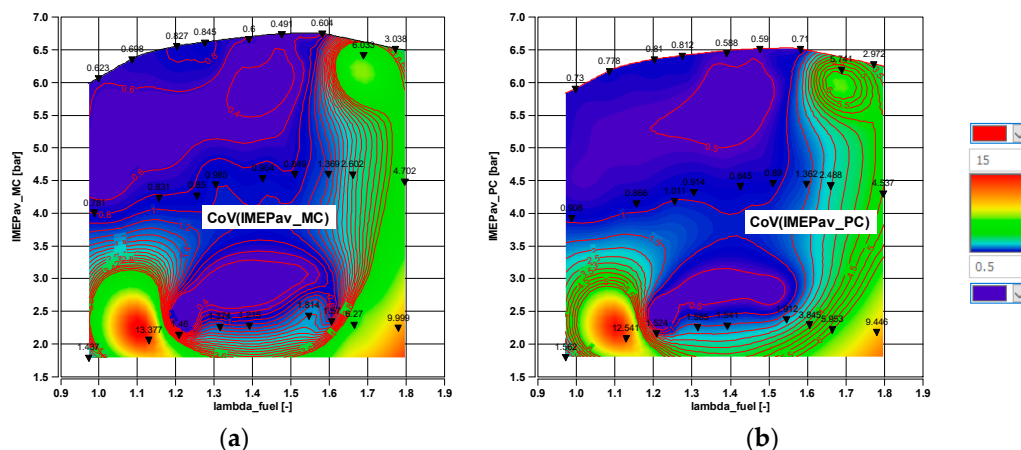


Figure 14. Maps of engine operation variability relative to the fuel mixture proportions: (a) in the main chamber; (b) in the prechamber.

In Figure 12, the CoV(IMEP) peaks at $\lambda = 1.1$ are visible, which are not visible in Figure 14. This is due to the way the map in Figure 14 was created, which contains only one point with a CoV(IMEP) value > 12%. Such a point does not provide grounds for determining large areas with high CoV(IMEP) values present at low engine loads. Several values in a similar load range already significantly affect the map image, CoV(IMEP) values at a high value of λ and high load (Figure 14b).

6. Initiation and Phases of the Combustion Process

Subsequent analyses of the combustion process required the precise determination of the start of combustion angle (SOC). Conventionally, in an SI engine, this angle can be assumed to be determined by the timing of ignition (or in a TJI engine with an active combustion chamber). Determining the ignition of the charge in the main chamber is not possible in the above-mentioned way. Thus, the SOC was calculated based on the pressure increment relative to the angle of the crankshaft. The largest value of the pressure increment was considered the start of combustion. A common way to determine this quantity is to use the equation:

$$\alpha_{SOC} = \alpha \text{ at } \left(\frac{dp}{d\alpha} \right)_{max} \tag{6}$$

where dp is the pressure change in the cylinder.

Equation (6) holds true for typical combustion systems (without a prechamber). In this situation, slightly different equations should be used. As shown in Figure 15, Equation (6) may result in an incorrect SOC calculation for the prechamber. This is mainly due to the rapid pressure increase in this chamber as a result of the ignition and combustion of the fuel dose.

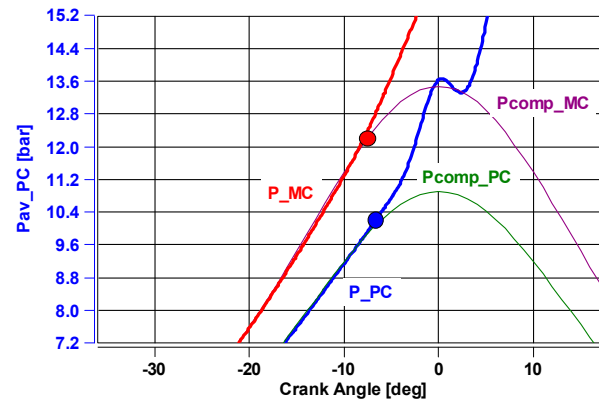


Figure 15. The method of determining the start of combustion at a given pressure in the main chamber and the prechamber of the tested engine (both pressures were presented on a much larger scale than in reality).

In order to avoid the incorrect determination of SOC_{PC} (start of combustion in prechamber), it was proposed that the start of combustion in both chambers should be defined as a 2% increase in the pressure value from the theoretical line of compression pressure in both chambers:

$$SOC_{MC} \rightarrow (P_{MC} - P_{MCcomp}) \geq 2\% \quad (7)$$

and

$$SOC_{PC} \rightarrow (P_{PC} - P_{PCcomp}) \geq 2\% \quad (8)$$

This approach made the possibility of incorrect SOC determination independent of the variable start of ignition (CoC regulation with a value of 8 deg aTDC). Having determined the SOC values (for both combustion chambers), they were related to the degree of how lean the mixture was (Figure 16a). The presented data showed that making the mixture leaner required increasing the ignition advance in order to obtain a constant value of CoC = 8 deg bTDC. It follows that the leaner the mixture, the greater the ignition advance angle value required. This relationship applied to each of the analyzed engine load values. It should be noted that increasing the engine load reduced the need to advance the ignition angle. With a load of IMEP = 4 bar and IMEP = 6 bar, the ignition advance was practically the same. The values of the start of combustion in the prechamber were about 3 deg higher than in the main chamber at $\lambda = 1$ and they increased with a leaner mixture. With large λ -values, the differences reached 4 deg CA. The increase in the difference between the start of combustion in the prechamber and the main chamber resulted from the leaner fuel mixture dose and the difficulty in flame development in those lean mixtures.

The full characteristics analysis of the difference in the start of combustion timing in both chambers is shown in Figure 16b. In general, it could be stated that the difference increased as the mixture became increasingly leaner, regardless of the engine load. The maximum differences were found for the leanest mixtures and a high load (at $\Delta > 4$ deg CA).

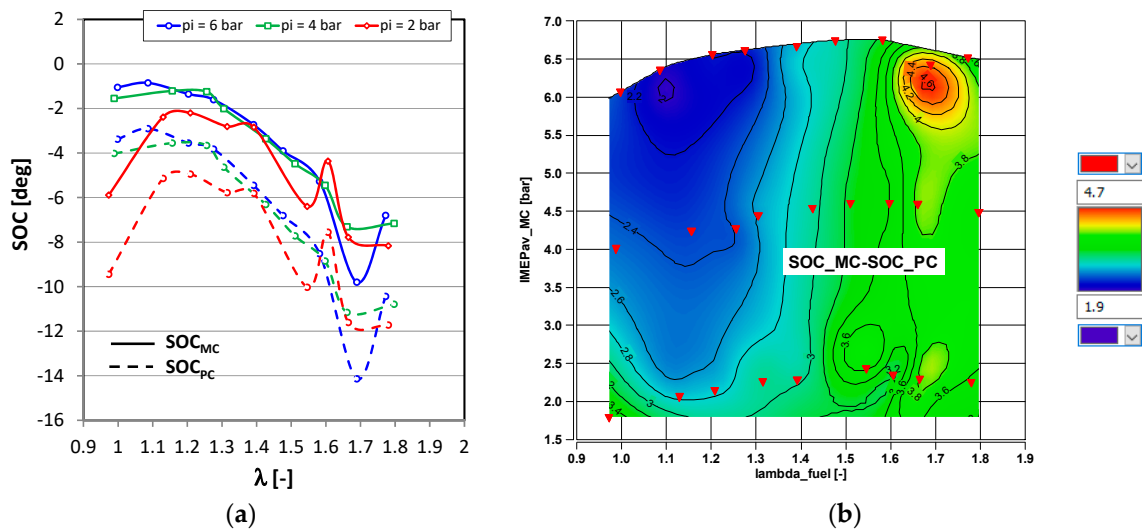


Figure 16. Changes in the start of combustion (SOC) due to engine load and mixture composition: (a) SOC changes in both chambers; (b) a map of the differences in the ignition start in the prechamber and the main chamber.

The combustion center calculated as described in Equation (3) also allowed the determination of the 5% heat release (AI05) and 90% heat release (AI90) values. These values, once obtained in this way, allowed the determination of the first and second phases of combustion. The ratio of phase I to phase II made it possible to indicate the longer combustion phase. The comparison of the combustion phases in relation to the mixture composition showed that the first phase was longer than the second (Figure 17a). Only at the smallest load value of IMEP = 2 bar and at $\lambda = 1$ was the duration of the first phase shorter than the second. With increasingly leaner mixtures, the duration of the first phase of combustion rose. This was mainly due to the prechamber mixture becoming leaner, resulting in impeded flame development. The above also caused a slower discharge of the burning mixture into the main chamber. A decrease in the duration of the first phase was observed at a high engine load. The reflection of this phenomenon was also observed in the full characteristics analysis (Figure 17b). In the area of high load and high value of λ , an area with a limited duration of the first phase (less than 50%) was observed.

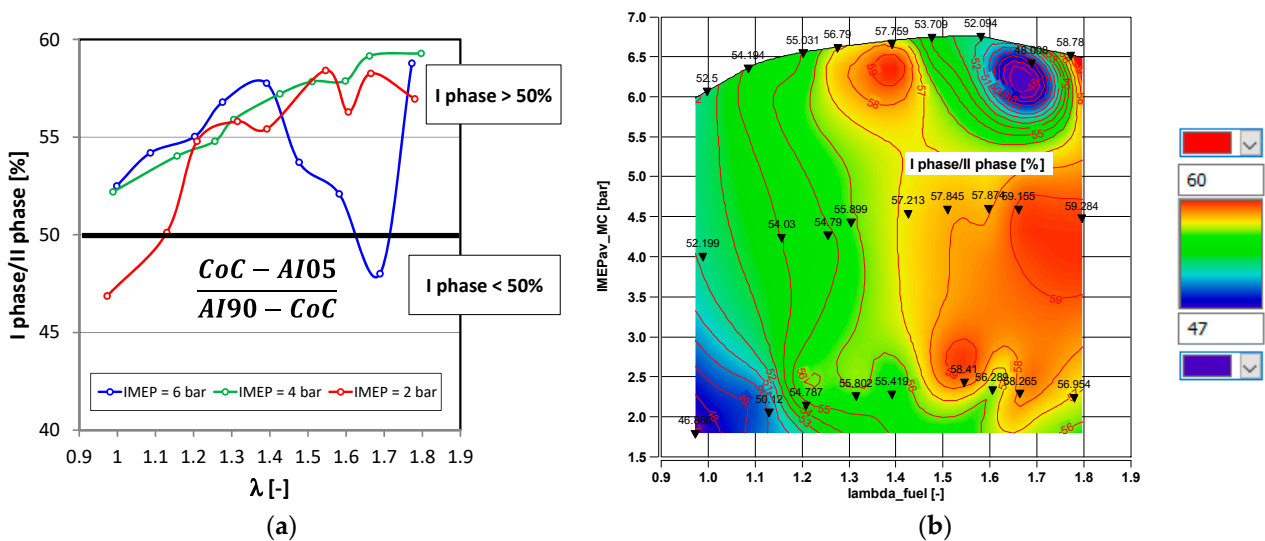


Figure 17. Analysis of the share of heat release time for the first and second combustion phases: (a) Percentage differences taking into account the load; (b) a map of percentage differences against changes in mixture composition and engine load.

7. Performance and Efficiency Analysis

The assessment of the combustion system was also based on determining the indicated efficiency of each analyzed point of engine operation, in accordance with the equations:

$$\eta_i = \frac{1}{q_0 \cdot L_{HV}} = \frac{1}{\frac{G_{MC} + G_{PC}}{N_i} \cdot L_{HV}} \quad (9)$$

where q_0 is a fuel dose, G is fuel consumption (in the main chamber G_{MC} and the prechamber G_{PC}), L_{HV} is the lower heat value and N_i is the indicated power, calculated using:

$$N_i = \frac{V_s \cdot p_i \cdot n}{\tau} \quad (10)$$

where V_s is the displacement of cylinder, n is the engine speed and $\tau = 2$ (4-stroke engine).

The indicated efficiency of the analyzed engine load values increased as the fuel mixture became leaner (Figure 18a). The maximum indicated efficiency was obtained in the range of $1.5 < \lambda < 1.6$. These values were independent of the engine load. It follows that the two-stage combustion system powered by a natural gas (pure methane) achieved the highest indicated efficiency of about 42% at a high load and $\lambda = 1.5$. This means that despite the mixture being leaner, it was possible to obtain the highest efficiency of the whole system. The engine operation at low load also achieved the highest efficiency ($\eta_i = 34.5\%$) at $\lambda = 1.5$. After exceeding the value of $\lambda > 1.6$ at each load value, the indicated engine efficiency decreased. This means that the prechamber used in the tests enabled the combustion of lean mixtures with high combustion efficiency for the value of $\lambda = 1.5$.

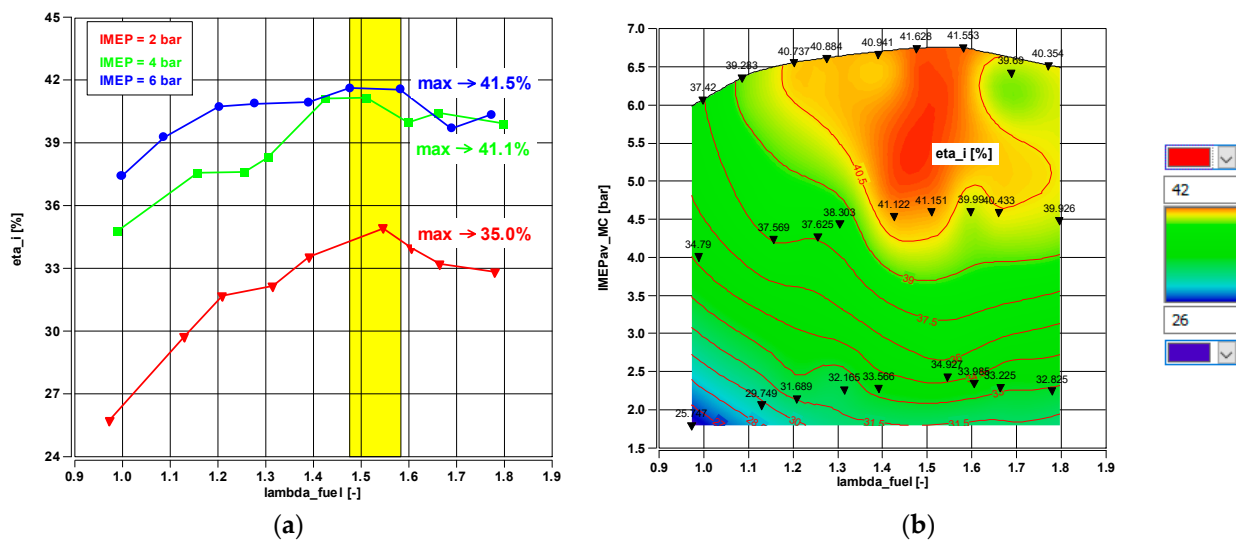


Figure 18. Evaluation of engine indicated efficiency: (a) as a function of mixture composition; (b) as a map of load characteristics and excess air coefficient.

The map of engine characteristics showed an increase in the indicated efficiency with increasing engine load. This means that the analyzed two-stage combustion system was more efficient than the traditional combustion system by about 8 percentage points at low loads. However, this efficiency was also higher for high load values: an increase of 5 percentage points (Figure 18b).

The presented analyses showed that the two-stage combustion system can be a valuable alternative to the conventional fuel supply and combustion system. A certain level of its complexity (two fuel supply systems and additional injectors) is compensated by the possible fuel savings.

8. Conclusions

The two-stage combustion system presented in the article showed advantages in relation to the traditional system:

- increasing the excess air ratio with the opening of the throttle at a constant fuel rate increased the value of the indicative mean effective pressure;
- at low loads, it allowed the increase in the indicated efficiency of the engine up to 36% at $\lambda = 1.5$ (about eight percentage points more in relation to the traditional combustion system at $\lambda = 1.0$);
- at high loads, the engine efficiency reached a value of about 42% at $\lambda = 1.5$ (increase in efficiency of about five percentage points in relation to the traditional combustion system at $\lambda = 1.0$).

A detailed analysis of the two-stage combustion system resulted in the following statements being made:

- the variability of engine operation in the range $\lambda < 1.6$ was below 2%, regardless of the load. It increased rapidly after exceeding $\lambda > 1.6$ and reached values around $\text{CoV(IMEP)} = 10\%$;
- the combustion of lean mixtures at the level of $\lambda = 1.6$ enabled the obtention of higher values of average indicated pressure; further increasing the excess air ratio lowered the quality of the combustion process;
- lean mixture combustion caused the specific fuel consumption to be much lower than 200 g/kWh. The lowest value of g_i was obtained in the range of $1.5 < \lambda < 1.6$;
- the start of combustion in the prechamber was 3–4 deg CA earlier than in the main chamber; this was due to the start of combustion in the prechamber and inter-chamber throttling;
- the combustion process analysis indicated the extension of the first combustion phase as the mixture became leaner.

Further work on the two-stage combustion system will be carried out towards obtaining and using increasingly leaner mixtures, which can be carried out using hydrogen fuel. Its use is associated with a further increase in combustion efficiency, while also keeping the increased emission of nitrogen oxides under control.

Author Contributions: Conceptualization, I.P. and F.S.; methodology, I.P. and F.S.; software, I.P. and F.S.; validation, I.P. and F.S.; formal analysis, I.P. and F.S.; investigation, I.P. and F.S.; resources, I.P. and F.S.; data curation, I.P. and F.S.; writing—original draft preparation, I.P. and F.S.; writing—review and editing, I.P. and F.S.; visualization, I.P. and F.S.; supervision, I.P. and F.S.; project administration, I.P. and F.S.; funding acquisition, I.P. and F.S. All authors have read and agreed to the published version of the manuscript.

Funding: This research received no external funding.

Institutional Review Board Statement: Not applicable.

Informed Consent Statement: Not applicable.

Data Availability Statement: The data presented in this study are available on request from the corresponding author.

Conflicts of Interest: The authors declare no conflict of interest.

References

1. (EC) No 443/2009; Regulation (EC) No 443/2009 of the European Parliament and of the Council of 23 April 2009 Setting Emission Performance Standards for New Passenger Cars as Part of the Community's Integrated Approach to Reduce CO₂ Emissions from Light-Duty Vehicles. The European Parliament: Strasbourg, France; The Council of the European Union: Brussels, Belgium, 2009. Available online: <http://data.europa.eu/eli/reg/2009/443/2018-05-17> (accessed on 17 December 2022).
2. (EU) No 510/2011; Regulation (EU) No 510/2011 of the European Parliament and of the Council of 11 May 2011 Setting Emission Performance Standards for New Light Commercial Vehicles as Part of the Union's Integrated Approach to Reduce CO₂ Emissions from Light-Duty Vehicles. The European Parliament: Strasbourg, France; The Council of the European Union: Brussels, Belgium, 2011. Available online: <http://data.europa.eu/eli/reg/2011/510/2019-07-08> (accessed on 17 December 2022).
3. Meng, Z.; Liu, Z.; Liu, J. Investigation of in-cylinder combustion deterioration of diesel engines in plateau regions. *Fuel* **2022**, *324*, 124824. [[CrossRef](#)]
4. Automobile Manufacturers' Association. *2022 Progress Report. Making the Transition to Zero-Emission Mobility. Enabling Factors for Alternatively-Powered Cars and Vans in the European Union*. European; European Automobile Manufacturers Association: Brussels, Belgium, June 2022. Available online: https://www.acea.auto/files/ACEA_progress_report_2022.pdf (accessed on 17 December 2022).
5. (EU) No 2019/631; Regulation (EU) No 2019/631 of the European Parliament and of the Council of 17 April 2019 Setting CO₂ Emission Performance Standards for New Passenger Cars and for New Light Commercial Vehicles, and Repealing Regulations (EC) No 443/2009 and (EU) No 510/2011 (Recast) (Text with EEA Relevance). The European Parliament: Strasbourg, France; The Council of the European Union: Brussels, Belgium, 2019. Available online: <http://data.europa.eu/eli/reg/2019/631/2021-12-02> (accessed on 17 December 2022).
6. Kraft, M.; Maigaard, P.; Mauss, F.; Christensen, M.; Johansson, B. Investigation of combustion emissions in a homogeneous charge compression injection engine: Measurements and a new computational model. *Proc. Combust. Inst.* **2000**, *28*, 1195–1201. [[CrossRef](#)]
7. Kale, A.V.; Krishnasamy, A. Experimental study of homogeneous charge compression ignition combustion in a light-duty diesel engine fueled with isopropanol–gasoline blends. *Energy* **2023**, *264*, 126152. [[CrossRef](#)]
8. Liu, J.; Yang, F.; Wang, H.; Ouyang, M. Numerical study of hydrogen addition to DME/CH₄ dual fuel RCCI engine. *Int. J. Hydrogen Energy* **2012**, *37*, 8688–8697. [[CrossRef](#)]
9. Kale, A.V.; Krishnasamy, A. Experimental optimization of homogeneous charge compression ignition through fuel modifications and a relative comparison with reactivity controlled compression ignition. *Energy Convers. Manag.* **2023**, *276*, 116439. [[CrossRef](#)]
10. Zheng, M.; Mulenga, M.C.; Reader, G.T.; Wang, M.; Ting, D.S.-K.; Tjong, J. Biodiesel engine performance and emissions in low temperature combustion. *Fuel* **2008**, *87*, 714–722. [[CrossRef](#)]
11. Wang, D.; Zhang, J.; Li, Y.; Yang, Z.; Shi, Z.; Lou, Y. Experimental investigation of transition process from LTC to ITC and HTC during diesel spray combustion at low ambient temperatures. *Fuel* **2023**, *333*, 126372. [[CrossRef](#)]
12. Akihama, K.; Takatori, Y.; Inagaki, K.; Sasaki, S.; Dean, A.M. Mechanism of the smokeless rich diesel combustion by reducing temperature. In *SAE Technical*; SAE International: Warrendale, PA, USA, 2001. [[CrossRef](#)]
13. Dec, J.E. Advanced compression-ignition engines—Understanding the in-cylinder processes. *Proc. Combust. Inst.* **2009**, *32*, 2727–2742. [[CrossRef](#)]
14. Ahmadi, R.; Hosseini, S.M. Numerical investigation on adding/substituting hydrogen in the CDC and RCCI combustion in a heavy duty engine. *Appl. Energ.* **2018**, *213*, 450–468. [[CrossRef](#)]
15. Hua, J.; Zhou, L.; Gao, Q.; Feng, Z.; Wei, H. Influence of pre-chamber structure and injection parameters on engine performance and combustion characteristics in a turbulent jet ignition (TJI) engine. *Fuel* **2021**, *283*, 119236. [[CrossRef](#)]
16. Mastorakos, E.; Allison, P.; Giusti, A.; De Oliveira, P.; Benekos, S.; Wright, Y.; Frouzakis, C.; Boulouchos, K. Fundamental aspects of jet ignition for natural gas engines. *SAE Int. J. Engines* **2017**, *10*, 2429–2438. [[CrossRef](#)]
17. Bueschke, W.; Szwajca, F.; Wislocki, K. Experimental Study on Ignitability of Lean CNG/Air mixture in the multi-stage cascade engine combustion system. In *SAE Technical*; SAE International: Warrendale, PA, USA, 2020. [[CrossRef](#)]
18. Pielecha, I.; Cieslik, W.; Wislocki, K. Optimization of two-stage combustion system fueled by lean-burn compressed natural gas mixtures for light-duty vehicle engines. *SAE Int. J. Engines*. **2020**, *13*, 503–519. [[CrossRef](#)]
19. Bueschke, W.; Skowron, M.; Szwajca, F.; Wislocki, K. Flame propagation velocity in 2-stage gas combustion system applied in SI engine. *IOP Conf. Ser. Mater. Sci. Eng.* **2018**, *421*, 042009. [[CrossRef](#)]
20. Bunce, M.; Blaxill, H.; Peters, N.; Subramanyam, S.K.P.; Cooper, A.; Bassett, M. Pre-chamber combustors: An enabling technology for high efficiency, low CO₂ engine operation. In *Engines and Fuels for Future Transport*; Kalghatgi, G., Agarwal, A.K., Leach, F., Senecal, K., Eds.; Springer: Singapore, 2022. [[CrossRef](#)]
21. Sens, M.; Binder, E. Pre-chamber ignition as a key technology for future powertrain fleets. *MTZ Worldw.* **2019**, *80*, 44–51. [[CrossRef](#)]
22. Soltic, P.; Hilfiker, T. Efficiency and raw emission benefits from hydrogen addition to methane in a prechamber-equipped engine. *Int. J. Hydrogen Energy* **2020**, *45*, 23638–23652. [[CrossRef](#)]
23. Liu, P.; Zhong, L.; Zhou, L.; Wei, H. The ignition characteristics of the pre-chamber turbulent jet ignition of the hydrogen and methane based on different orifices. *Int. J. Hydrogen Energy* **2021**, *46*, 37083–37097. [[CrossRef](#)]

24. Duan, X.; Liu, J.; Yuan, Z.; Guo, G.; Liu, Q.; Tang, Q.; Deng, B.; Guan, J. Experimental investigation of the effects of injection strategies on cycle-to-cycle variations of a DISI engine fueled with ethanol and gasoline blend. *Energy* **2018**, *165*, 455–470. [[CrossRef](#)]
25. Pielecha, I.; Wisłocki, K.; Cieślak, W.; Bueschke, W.; Skowron, M.; Fiedkiewicz, L. Application of IMEP and MBF50 indexes for controlling combustion in dual-fuel reciprocating engine. *Appl. Therm. Eng.* **2018**, *132*, 188–195. [[CrossRef](#)]
26. Szwejca, F.; Wisłocki, K. Thermodynamic cycles variability of TJI gas engine with different mixture preparation systems. *Combust. Engines* **2020**, *181*, 46–52. [[CrossRef](#)]
27. Wang, L.; Liu, J.; Ji, Q.; Sun, P.; Li, J.; Wei, M.; Liu, S. Experimental study on the high load extension of PODE/methanol RCCI combustion mode with optimized injection strategy. *Fuel* **2022**, *314*, 122726. [[CrossRef](#)]
28. Sementa, P.; de Vargas Antolini, J.B.; Tornatore, C.; Catapano, F.; Vaglieco, B.M.; López Sánchez, J.J. Exploring the potentials of lean-burn hydrogen SI engine compared to methane operation. *Int. J. Hydrogen Energy* **2022**, *47*, 25044–25056. [[CrossRef](#)]
29. Beatrice, C.; Belgiorno, G.; Di Blasio, G.; Mancaruso, E.; Sequino, L.; Vaglieco, B.M. Analysis of a prototype high-pressure “hollow cone spray” diesel injector performance in optical and metal research engines. In *SAE Technical*; SAE International: Warrendale, PA, USA, 2017. [[CrossRef](#)]
30. Vitek, O.; Macek, J.; Klíma, J.; Vacek, M. Optimization of 2-stage turbocharged gas SI engine under steady state operation. *J. Middle Eur. Constr. Des. Cars* **2017**, *15*, 9–36. [[CrossRef](#)]
31. Di Blasio, G.; Belgiorno, G.; Beatrice, C.; Fraioli, V.; Migliaccio, M. Experimental evaluation of compression ratio influence on the performance of a dual-fuel methane-diesel light-duty engine. *SAE Int. J. Engines* **2015**, *8*, 2253–2267. [[CrossRef](#)]
32. Weißner, M.; Beger, F.; Schüttenhelm, M.; Tallu, G. Lean-burn CNG engine with ignition chamber: From the idea to a running engine. *Combust. Engines* **2019**, *176*, 3–9. [[CrossRef](#)]
33. Ravaglioli, V.; Moro, D.; Serra, G.; Ponti, F. MFB50 on-board evaluation based on a zero-dimensional ROHR model. In *SAE Technical*; SAE International: Warrendale, PA, USA, 2011. [[CrossRef](#)]
34. Wagner, R.M.; Drallmeier, J.A.; Daw, C.S. Prior-cycle effects in lean spark ignition combustion—Fuel/air charge considerations. In *SAE Technical*; SAE International: Warrendale, PA, USA, 1998. [[CrossRef](#)]
35. Zhang, M.; Hong, W.; Xie, F.; Liu, Y.; Su, Y.; Li, X.; Liu, H.; Fang, K.; Zhu, X. Effects of diluents on cycle-by-cycle variations in a spark ignition engine fueled with methanol. *Energy* **2019**, *182*, 1132–1140. [[CrossRef](#)]
36. Chen, Y.; Dong, G.; Mack, J.H.; Butt, R.H.; Chen, J.-Y.; Dibble, R.W. Cyclic variations and prior-cycle effects of ion current sensing in an HCCI engine: A time-series analysis. *Appl. Energy* **2016**, *168*, 628–635. [[CrossRef](#)]

Disclaimer/Publisher’s Note: The statements, opinions and data contained in all publications are solely those of the individual author(s) and contributor(s) and not of MDPI and/or the editor(s). MDPI and/or the editor(s) disclaim responsibility for any injury to people or property resulting from any ideas, methods, instructions or products referred to in the content.